ELSEVIER

Contents lists available at ScienceDirect

Icarus

journal homepage: www.elsevier.com/locate/icarus



Letter

Phosphates reveal high pH ocean water on Enceladus

Christopher R. Glein*, Ngoc Truong

Space Science Division, Space Sector, Southwest Research Institute, 6220 Culebra Road, San Antonio, TX 78238-5166, United States



ARTICLE INFO

Keywords:
Cosmochemistry
Enceladus
Interiors
Satellites, composition
Volcanism

ABSTRACT

Enceladus offers our best opportunity for exploring the chemistry of an ocean on another world. Here, we perform geochemical modeling to show how the distribution of phosphate species found in ice grains from Enceladus's plume provides a very straightforward constraint on the pH of the host solution. The ratio of HPO₄/ PO₄ species serves as a pH indicator. We find evidence of moderately alkaline water (pH 10.1-11.6)—significantly more alkaline than current estimates (~8-9) of the pH of Enceladus's ocean. Nevertheless, the pH range from phosphates is consistent with the CO₂/H₂O ratio measured in the plume if CO₂ exsolves from ocean water according to its equilibrium solubility. A simple energy balance can be used to quantify volatile fractionation during gas transport inside Enceladus's tiger stripes; we deduce that ~83 % of water vapor is removed as ice during transport between the liquid-vapor interface and where gases exit the subsurface. We also explore how CO2 degassing may lead to an increase in the apparent pH of ocean water. We generate maps of allowed combinations of pH and dissolved inorganic carbon concentration of the source water for a wide range of scenarios. Our preferred interpretation, constrained by the observed heat flux, implies minimal CO₂ degassing from ocean water. Hence, the pH recorded by phosphates should closely approximate that of the ocean; our best estimate is pH ~10.6. Such a high pH seems to reflect a major role of silicates enriched in Na, Mg, or Fe(II) interacting extensively with ocean water. Silica nanoparticles would not form or would subsequently dissolve if the pH is too high (>10.5). The outgassing model presented here provides a new path to quantify the dissolved concentrations of volatile species.

1. Introduction

1.1. One variable to rule them all in aqueous geochemistry

The pH is a geochemical parameter that determines the stable forms of dissolved chemical species and the solubilities of minerals. It can also strongly influence the rates of mineral dissolution and the energetics of microbial metabolisms (Jin and Kirk, 2018). In field geochemistry, pH is one of the first measurements that is made to characterize the nature of aqueous solutions. The pH quantifies the acidity of a solution; it is defined as

$$pH = -\log a_{H^+} \tag{1}$$

where $a_{\rm H^+}$ designates the activity of H $^+$ referenced to the ideal dilute standard state on the molality (mol/kg H $_2$ O) scale at the temperature and pressure of interest.

Saturn's moon Enceladus has an ice-covered ocean that erupts into space, forming a plume of gases and ice grains (Hansen et al., 2006; Porco et al., 2006; Postberg et al., 2009; Thomas et al., 2016; Villanueva et al., 2023). This ocean is thought to be one of our best bets in the search for extraterrestrial life because its composition appears to make it habitable (Waite et al., 2009, 2017; Postberg et al., 2018, 2023; Ray et al., 2021; Xu et al., 2025), and the plume provides samples of the ocean without the need to dig or drill (Cable et al., 2021). Accordingly, considerable effort has gone into understanding the chemistry of Enceladus's ocean (Zolotov, 2007; Glein et al., 2018; Fifer et al., 2022; Ramírez-Cabañas et al., 2024). However, unlike on Earth where we can use a pH meter, we cannot directly determine pH on Enceladus. Various indirect approaches have been developed to estimate the pH, but they yield values spanning from weakly (pH ~8) to strongly (pH ~12) alkaline (Postberg et al., 2009; Glein et al., 2015; Hsu et al., 2015; Glein and Waite, 2020; Fifer et al., 2022).

E-mail address: christopher.glein@swri.org (C.R. Glein).

^{1.2.} pH is integral to Enceladus's ocean chemistry

^{*} Corresponding author.

Recently, a consensus has been building around an ocean pH of \sim 8–9 (Glein and Waite, 2020; Fifer et al., 2022). These researchers developed geochemical models of ocean chemistry based on different assumptions about how the process of forming the plume from ocean water containing salts and dissolved gases would fractionate materials between the ocean and plume. They then inferred pH ranges that would allow a consistent interpretation of Cassini data using their models. A weakly basic ocean seemed attractive because it was consistent with the pattern of pH-dependent peaks observed in mass spectra of salt-rich plume particles (Postberg et al., 2009), and with a hydrothermal interpretation for signatures of silica seen streaming from the Saturn system (Hsu et al., 2015). However, the analysis of mass spectra of salt-rich plume particles has advanced greatly (Postberg et al., 2021; Seaton et al., 2025) since the pioneering work of Postberg et al. (2009). We will return to the topic of hydrothermal silica in Section 4.2. The prevailing estimates for the pH of Enceladus's ocean may not be as well constrained as commonly perceived. If so, then there is a need for additional data.

1.3. Phosphate speciation as a novel indicator of pH

After the studies of Glein and Waite (2020) and Fifer et al. (2022), phosphate salts were discovered in ice grains from the plume. Postberg et al. (2023) found that observed mass spectra of phosphate-rich grains can be reproduced from laboratory mixtures with molar ratios of Na₂HPO₄/Na₃PO₄ between 2.5 and 25. They used a laser to disperse ions from a liquid-water beam containing these salts. This approach is meant to mimic impact ionization of salt-bearing ice grains analyzed in space (Klenner et al., 2019). The reported range of Na₂HPO₄/Na₃PO₄ ratios gave best matches to the peak pattern of three phosphate-bearing Nacluster cations identified in mass spectra of nine P-rich grains that were discovered in Saturn's Ering. It is fair to question the relevance of liquid experiments to solid ice particles; this topic is an active area of research (e.g., Burke et al., 2023). Nevertheless, we will interpret the observational constraint on the ratio of phosphate species using models of aqueous chemistry that do not involve brines or the precipitation of salts. A direct comparison between Postberg et al.'s (2023) liquid-based constraint and our models may be most appropriate. In any event, their constraint provides a new opportunity to test our understanding of the pH of Enceladus's ocean.

The phosphate system is a classic example of polyprotic acid-base equilibria. Aqueous phosphoric acid (H_3PO_4) is the starting point, followed by a series of acid dissociation reactions that terminate at the phosphate anion (PO_4^{-3}) :

$$H_3PO_4(aq) \rightleftharpoons H_2PO_4^-(aq) + H^+(aq)$$
 (2)

$$H_2PO_4^-(aq) \rightleftharpoons HPO_4^{-2}(aq) + H^+(aq)$$
 (3)

and

$$HPO_4^{-2}(aq) \rightleftharpoons PO_4^{-3}(aq) + H^+(aq)$$
 (4)

We can gain first-order insight into how the relative abundances of these phosphate species depend on pH by constructing a Bjerrum plot. Fig. 1 shows the behavior for an ideal solution based on thermodynamic data from Shock et al. (1989, 1997). In an ideal solution, all species have activities that equal their molalities (see Section 2). This assumption is known to diverge from reality as solutions become saltier. Nevertheless, starting with an ideal solution can be helpful to illustrate fundamental concepts of aqueous geochemistry. If we proceed on a provisional basis, then it is evident that, at pH \sim 8–9, the phosphate speciation should be dominated by HPO $_4^{-2}$ and H $_2$ PO $_4^{-}$, whereas PO $_4^{-3}$ should have a negligible abundance. This expectation is inconsistent with the phosphate speciation determined by Postberg et al. (2023). It appears that the pH needs to be higher to obtain the correct phosphate speciation. However, more detailed quantification using Fig. 1 would be ill-advised because these simple calculations do not account for salt effects. Therefore, the

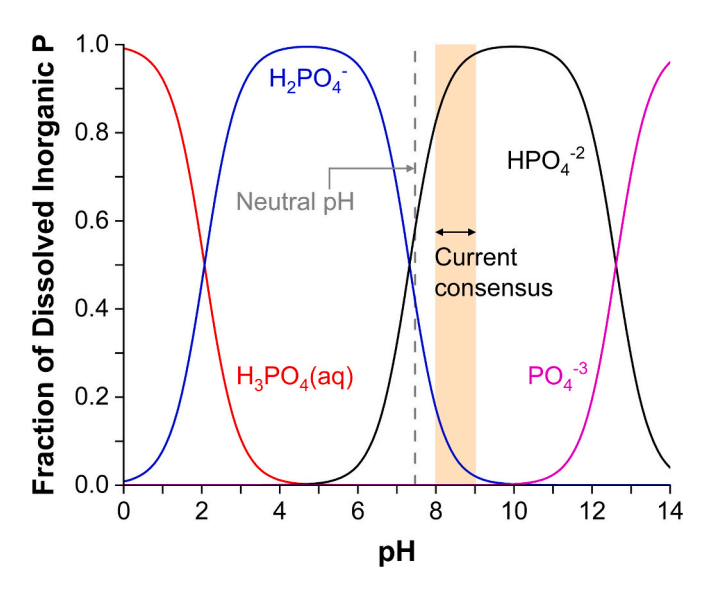


Fig. 1. How the ideal distribution of phosphate species changes with pH at $0\,^{\circ}$ C and 1 bar. The pH of neutral water at these conditions is indicated. Also indicated is the currently accepted range for the pH of Enceladus's ocean (Glein and Waite, 2020; Fifer et al., 2022).

main objective of this work is to constrain the pH using a more robust geochemical model of phosphate speciation on Enceladus. We will then explore how representative the "plume pH" is of the ocean below, and conclude with a few of the most important implications of a new pH range.

2. Modeling approach

Rxn. (4) is the key reaction that enables us to relate Postberg et al.'s (2023) constraint on the Na_2HPO_4/Na_3PO_4 ratio to solution pH. The law of mass action for the equilibrium constant (K) of this reaction can be written as shown below:

$$K_4 = \frac{a_{\text{PO}_4}^{-3} a_{\text{H}^+}}{a_{\text{HPO}_4}^{-2}} = \frac{\gamma_{\text{PO}_4}^{-3}}{\gamma_{\text{HPO}_4}^{-2}} \frac{m_{\text{PO}_4}^{-3}}{m_{\text{HPO}_4}^{-2}} a_{\text{H}^+}$$
 (5)

where a_i , γ_i , and m_i refer to the activity, activity coefficient, and molality of the ith species, respectively. To calculate the pH via Eq. (1), we can see that the concentration ratio of phosphate species is necessary but insufficient to evaluate Eq. (5)—we must also know the ratio of activity coefficients. The latter is one place where salt effects come into play.

Eq. (5) shows that activity coefficients are needed to solve the pH problem, and these correction factors are expected to vary with the salinity of phosphate-bearing fluids. Therefore, to constrain pH, we need to set limits on salinity. Postberg et al. (2009) provided the first constraints on the salt chemistry of plume ice grains, but they have been making improvements since then (Postberg et al., 2021). Based on the latest, publicly presented results, we have defined salt-poor and salt-rich endmembers (Table S1).

Our geochemical model is of the $Na_2O-K_2O-CO_2-H_3PO_4-HCl-HBr-H_2O$ system, which includes all observed salt species (Postberg et al., 2009, 2021, 2023). While the concentration of dissolved Ca can be expected to be an important controller of the concentration of dissolved P, the concentration of dissolved Ca does not need to be specified in a model of aqueous speciation only (i.e., no seafloor minerals) when we already know the concentration of dissolved P (Postberg et al., 2023). To the best of our knowledge, Ca has never been detected in plume or E-ring ice grains from Enceladus—this lack of detection is broadly consistent with the presence of abundant P. We compute the system's speciation over a reaction path of varying pH using the React app in The Geochemist's Workbench 2023. Because salty plume grains will record

conditions near the ice-liquid interface, we assume that the freezing temperature of water is most appropriate and the corresponding pressure is low. Our model conditions are 0 °C and 1 bar $(10^5 \text{ Pa})^1$ The overall approach is similar to that of Glein et al. (2015), except here we use an updated thermodynamic database. Our new database was generated from the default database in the PyGeochemCalc package (Awolayo and Tutolo, 2022). We added 13 species to this database that may be important to the speciation on Enceladus: NaCO $_3^-$, NaHCO $_3$ (aq), and H $_2$ CO $_3$ (aq) from the Deep Earth Water model (Huang and Sverjensky, 2019), and a set of Na and K phosphate complexes from Daniele et al. (1991) (see Thermodynamic data file). In our React calculations, activity coefficients of ionic species are computed using an extended Debye-Hückel equation (Helgeson, 1969), since the plume ice is salty but is not a brine.

We perform additional calculations using React to explore the chemical consequences of CO_2 degassing from carbonate-bearing fluids on Enceladus. The same thermodynamic database is used. This scenario assumes that pre-degassed ocean water could have a lower pH and higher dissolved inorganic carbon (DIC) concentration than those represented by plume salts. We seek to constrain initial ocean conditions of pH-DIC that would be allowed as CO_2 is progressively removed from the source fluid. To keep the focus on these key unknowns, in this set of calculations, we consider intermediate values for the following input parameters: CI = 0.2 molal (m), dissolved inorganic phosphorus (DIP) = 0.004 m (see Table S1), and K/Na = 1/16 (i.e., CI chondritic; Lodders, 2021).

3. Results and discussion

3.1. High pH yields the observed phosphate speciation

Enceladus's observed phosphate speciation is indicative of a pH between 10.1 and 11.6 (Fig. 2). The overall uncertainty due to observed salts is \sim 0.5 pH units, with the salt-rich endmember shifted to lower pH. It should be noted that our calculations account for the effects of bulk salts measured in frozen ocean water (Postberg et al., 2009, 2011, 2021, 2023). These ice grains are salty but do not appear to be brines. However, one could imagine residual liquid to keep respeciating until freezing is complete. This type of evolution may allow the pH to be lower than what we calculated (Fig. 2). On the other hand, salt effects may not be extrapolated so simply into the highly concentrated regime owing to ion association and other complications. There is also the question of how much of the chemical system is kinetically responsive once it is almost totally frozen (Fox-Powell and Cousins, 2021). Such complexity introduces uncertainty that is at present difficult to quantify, but we would be surprised if the pH were to go below \sim 9. A large change in a_{H^+} would be needed since pH is expressed on a logarithmic scale. Future work is required to test this suspicion. Alternatively, because Postberg et al. (2023) did not use brines when they constrained the Na₂HPO₄/ Na₃PO₄ ratio, a model of brine chemistry may not be needed to interpret their constraint.

Our speciation calculations provide other details about the chemical nature of Enceladean ocean water. Sodium and chloride ions are found to dominate the distribution of species, and the dominant form of DIC is carbonate in one form or another (see Fig. S1b, S1d). The chemistry of these solutions bears a striking resemblance to salts found in Ryugu and Bennu samples (Matsumoto et al., 2024; McCoy et al., 2025). It is intriguing to ponder whether the Bennu parent body could serve as an analog of Enceladus. In addition to hosting Na-rich chloride, carbonate, and phosphate salts, Bennu samples also contain abundant ammonia,

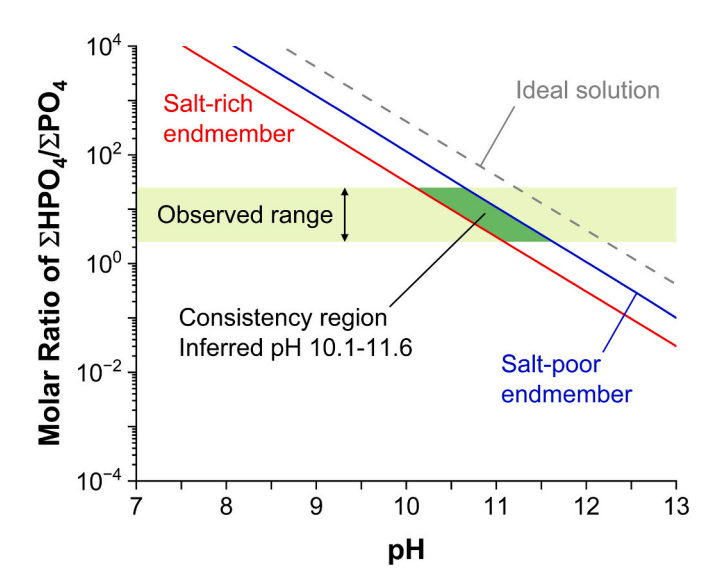


Fig. 2. Using the observed ratio of HPO₄ and PO₄ species (Postberg et al., 2023) to deduce the pH of their host solution. Summation signs indicate all dissolved species containing HPO₄ or PO₄, including ion pairs such as NaHPO $_4$. Red and blue lines show ratios that are predicted after the compositions given in Table S1 are speciated as a function of pH at 0 °C and 1 bar. The ideal speciation shown in Fig. 1 is represented by the gray dashed line. An ideal solution ignores the effects of salts on species activities, as ions in such a solution are assumed to behave as if they were in an infinitely dilute solvent. The dark green region shows where both constraints (Σ HPO₄/ Σ PO₄ ratio and salinity) converge. (For interpretation of the references to color in this figure legend, the reader is referred to the web version of this article.)

methylamine, and acetic acid (Glavin et al., 2025)—similar to materials erupted from Enceladus (Khawaja et al., 2019; Peter et al., 2024). However, this analogy does not mean that their detailed speciations should be the same. As an example, Bennu's soluble phosphates contain both Na and Mg (McCoy et al., 2025), while those at Enceladus have been observed to contain only Na as the counterion (Postberg et al., 2023). Materials from Bennu also attest to desiccation, whereas Enceladus currently has a deep ocean of water. Nevertheless, we suggest that it may be fruitful to further explore their geochemical relationships to better understand pathways of water-rock-organic evolution in the outer solar system.

We find that salts shift and may enter the speciation of DIP on Enceladus (Fig. S1a, S1c). For example, NaHPO $_4^-$ can be the dominant form of P depending on the concentration of sodium. We also find a salinity range of 5.1–55 g/kg solution, which can be compared to a minimum of ~20 % to permit whole-ocean convection (Zeng and Jansen, 2021). As a result, it seems premature to conclude that Enceladus's ocean should be stratified (Ames et al., 2025). By combining our speciation with the model of McCleskey et al. (2012), the electrical conductivity of these ocean samples can be estimated (Castillo-Rogez et al., 2022). The predicted range is 0.83–7.5 S/m. These values can aid efforts to interpret magnetic measurements at Enceladus (Saur et al., 2024).

3.2. Equilibrium exsolution can explain a high pH

Our new pH range is significantly higher than the current consensus of \sim 8–9 (Glein and Waite, 2020; Fifer et al., 2022). Those models employed different assumptions, but they both invoked kinetic control of processes linking the ocean and plume compositions. In contrast, Glein et al. (2015) showed that equilibrium processes occurring during volatile transport can lead to the inference of a high pH fluid. However, their pH values (10.8–13.5) may be too high compared with the range implied by the observed phosphate speciation. Here, we seek to

 $^{^1}$ The most widely used pressure in thermodynamic databases at temperatures below 100 $^{\circ}\text{C}$ is 1 bar. Nevertheless, equilibria between aqueous species are negligibly affected by a small pressure difference between the triple-point pressure ($\sim\!6.1$ mbar) and 1 bar.

determine whether an updated version of their model can produce more consistent results.

Glein et al. (2015) pointed out that water vapor condensation causes other gases to be enriched in the mixture that emerges from the subsurface of Enceladus. Some water vapor freezes out during transport because of a temperature decrease between the liquid water source of the plume and the local environment where jetting occurs (Goguen et al., 2013). The icy cracks connecting Enceladus's ocean and surface can be thought of as giant distillation columns. We can simplify the problem of accounting for the condensation of water vapor in reconstructing the composition of the gas phase in equilibrium with Enceladean ocean water by assuming that more-volatile gases do not condense during transport (see Section 3.3.1.2). We focus on CO_2 here since its partial pressure can be related to pH through carbonate chemistry. The mass balance of CO_2 can be written as

$$\dot{n}_{\rm H_2O,LVE} \times ({\rm CO_2/H_2O})_{\rm LVE} \approx \dot{n}_{\rm H_2O,SVE} \times ({\rm CO_2/H_2O})_{\rm SVE}$$
 (6)

where $\dot{n}_{\rm H_2O}$ represents a flow rate of water vapor in moles per second. Our notation defines two key regions of equilibrium (Fig. 3). Liquid-

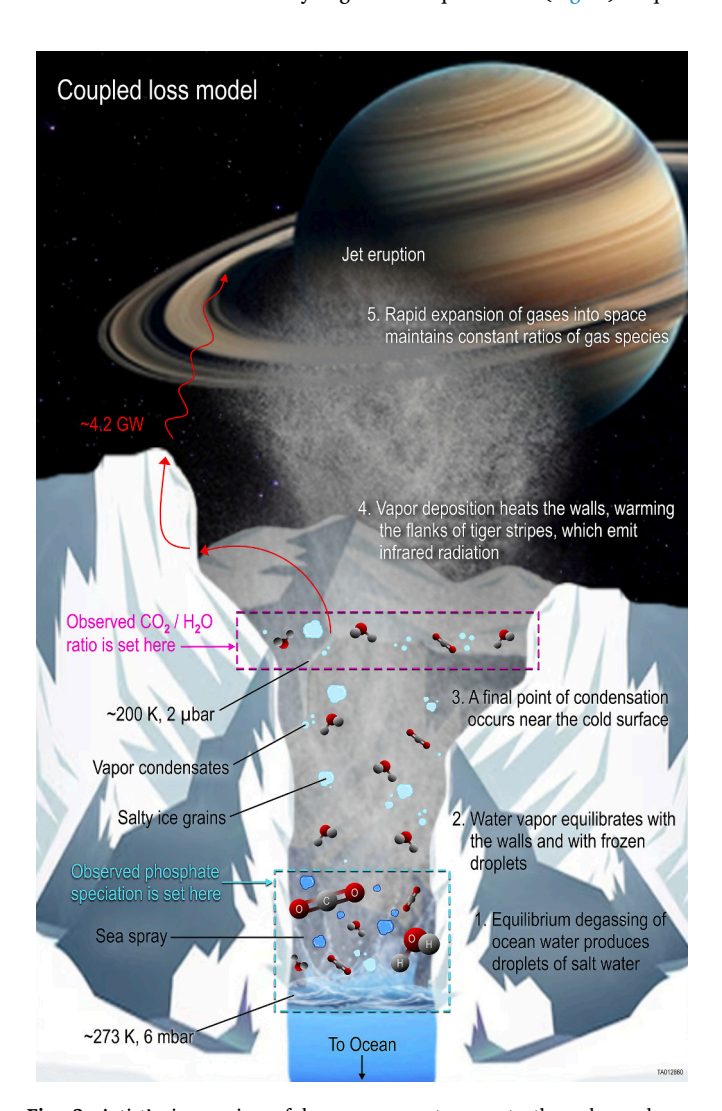


Fig. 3. Artist's impression of how ocean water erupts through cracks on Enceladus. This image highlights processes that affect compositional signatures of erupted materials. Our representation follows from others in the literature (e. g., Spencer et al., 2018; Khawaja et al., 2019), although ours adds details that are clarified in the present paper. By understanding key processes of fractionation, we can properly interpret chemical observations and use them to constrain the chemistry of the input ocean water. Dimensions are not to scale. Credit: A.J. Galaviz (SwRI).

vapor equilibrium (LVE) corresponds to the region where a liquid water solution is outgassed. Exsolved gases then traverse through cracks in Enceladus's ice shell until a final point of solid-vapor equilibrium (SVE) is reached before the gases erupt at the surface. Eq. (6) is a corrected version of Glein et al.'s (2015) mass balance from Fifer et al. (2022). The latter authors pointed out that the flow rate rather than the density of water vapor should serve as the scaling factor of the mixing ratio, as the cross-sectional area and velocity of the flow most likely change between the bottom and top of gas-filled cracks. The molar ratio of gaseous CO_2/H_2O at the bottom is given by

$$(\text{CO}_2/\text{H}_2\text{O})_{\text{LVE}} \approx \frac{\dot{n}_{\text{H}_2\text{O},\text{SVE}}}{\dot{n}_{\text{H}_2\text{O},\text{LVE}}} \times (\text{CO}_2/\text{H}_2\text{O})_{\text{SVE}}$$
 (7)

If it is then recognized that

$$\left(\text{CO}_2/\text{H}_2\text{O}\right)_{\text{LVE}} = \frac{p_{\text{CO}_2,\text{LVE}}}{p_{\text{H}_2\text{O},\text{LVE}}} \tag{8}$$

one can derive an equation for the partial pressure of ${\rm CO}_2$ at the liquid-vapor interface of the crack:

$$logp_{\text{CO}_2,\text{LVE}} \approx logp_{\text{H}_2\text{O},\text{LVE}} + log\left(\frac{\dot{n}_{\text{H}_2\text{O},\text{SVE}}}{\dot{n}_{\text{H}_2\text{O},\text{LVE}}}\right) + log(\text{CO}_2/\text{H}_2\text{O})_{\text{SVE}} \tag{9}$$

This equation can be evaluated by assuming that the partial pressure of $\rm H_2O$ at the point of LVE is the triple-point pressure of ~ 0.0061 bar, and the $\rm CO_2/H_2O$ ratio is quenched at this point so that the plume value (~ 0.005 ; Peter et al., 2024) can be used. However, we also need to know the fraction of water vapor that condenses between the bottom and top of gas-filled cracks.

Fifer et al. (2022) address the problem of water vapor condensation by implementing a complex model of heat and mass transfer from Nakajima and Ingersoll (2016). Their model tracks the flow of water vapor in gas-filled cracks. In this work, we opt for a much simpler approach. We will first consider an endmember in which no water vapor condenses to derive an upper limit on $p_{\mathrm{CO}_2,\mathrm{LVE}}$ (see below). Then, in a later section (see Section 3.3.1.2), we will show that an energy conservation argument can be made to circumvent modeling of fluid dynamics, which depend on unknown details of crack geometry such as depth and width (Nakajima and Ingersoll, 2016). From the perspective of volatile fractionation, such modeling is unnecessary because all we need to know is the fraction of water vapor that condenses, which reflects initial and final states in the crack. We are not questioning the accuracy of Nakajima and Ingersoll's (2016) model compared to ours, and indeed, we expect to find a similar condensed fraction as they did since both models must satisfy the same constraints on the fluxes of water vapor and heat (e.g., Spencer et al., 2018; Hansen et al., 2020).

From Section 3.1, geochemical calculations that reproduce the observed phosphate speciation yield a range of CO2 partial pressures from $10^{-7.27}$ to $10^{-4.23}$ bar. We can set an independent upper limit on $p_{\rm CO_2,LVE}$ based on the $\rm CO_2/H_2O$ ratio in the plume gas. We calculate an upper limit of $10^{-4.5}$ bar using Eq. (9) with $\dot{n}_{\rm H_2O,SVE}/\dot{n}_{\rm H_2O,LVE}=1$ (i.e., no condensation of water vapor). This $p_{\text{CO}_2,\text{LVE}}$ is consistent with the observed phosphate speciation. Condensation of water vapor will lead to lower inferred values of $p_{\text{CO}_2,\text{LVE}}$ (see Section 3.3.1.2). Because our model of equilibrium between CO2 dissolved in ocean water and CO2 in the overlying gas phase gives a $p_{CO_2,LVE}$ range that agrees with the CO_2/H_2O ratio measured in Enceladus's plume (Peter et al., 2024), the assumption that this equilibrium is reached appears to be supported. Fifer et al. (2022) assumed instead that gas transfer across the liquid-vapor interface is not at a state of equilibrium but is determined by rates of diffusive transport. This assumption led them to infer that Enceladus's ocean water has a much higher p_{CO_2} than the gas phase adjacent to it (Fig. 3). However, such disequilibrium would imply a lower pH of ~8-9 that appears to be inconsistent with the observed phosphate speciation. All

forms of DIC contribute to CO_2 that is outgassed into the plume in our model. In the model of Fifer et al. (2022), outgassed CO_2 comes from dissolved CO_2 only. The likelihood of equilibrium being reached during outgassing provides an important constraint on the dynamical timescale of the eruptive process (it should not be too fast), which may have consequences for other aspects of the plume's chemistry, such as how different salts are segregated between ice grains (Postberg et al., 2021).

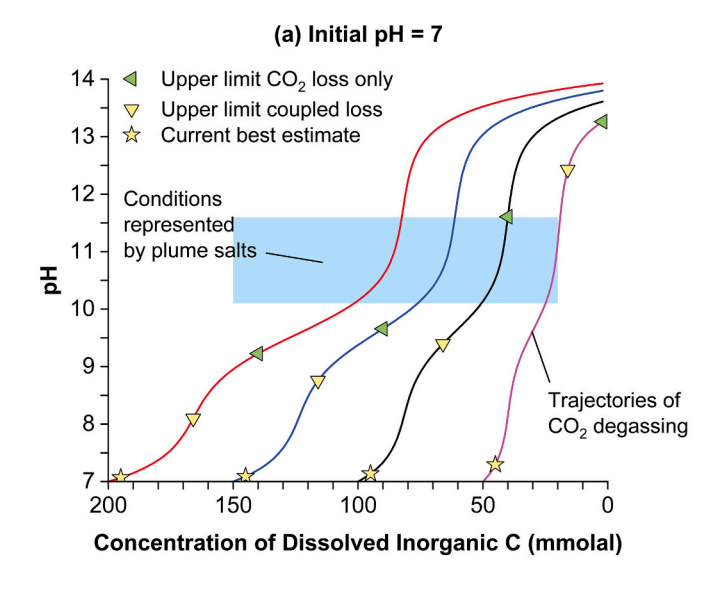
3.3. Plume pH versus ocean pH

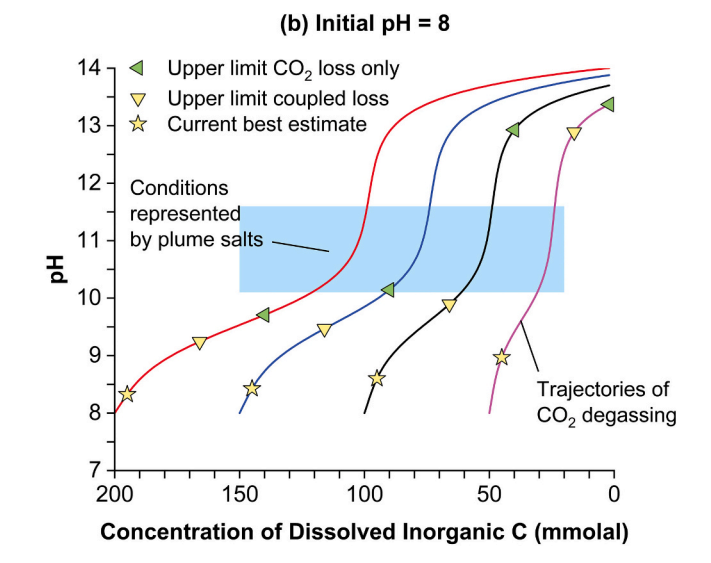
Does the high pH recorded by phosphate species reflect the bulk ocean of Enceladus, or does some process modify the pH? One process known to raise pH in natural waters on Earth is CO_2 degassing. Spring waters commonly degas CO_2 when they emerge from aquifers to Earth's surface, where the partial pressure of CO_2 is lower than it is underground (e.g., Choi et al., 1998). The surface of Enceladus is effectively a vacuum, so Enceladus's ocean water should degas CO_2 if it is brought close to the

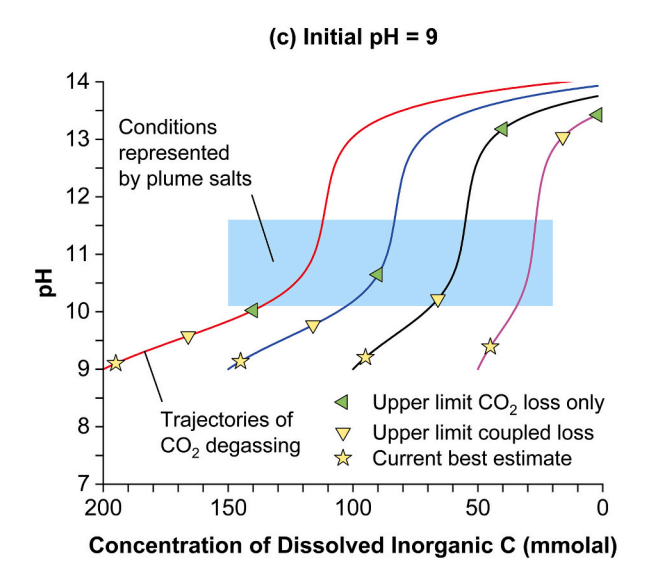
surface. In fact, CO_2 is one of the major plume gases (Peter et al., 2024). Respeciation after the removal of CO_2 (but before freezing) could increase the pH to an unknown extent, because CO_2 affects carbonate chemistry differently depending on whether it is dissolved in water or present in the gas phase. We need to understand this process to relate the pH determined from erupted droplets (see Section 3.1) to deeper ocean water.

Fig. 4 shows what would happen to the pH if solutions starting with various DIC concentrations and pH values were to undergo CO_2 removal. It can be seen that pH does indeed increase. It increases because CO_2 is a weak acid in water ("carbonic acid"), and the removal of an acid makes a solution more basic. In terms of the main reactions occurring near the inferred pH range for Enceladus, at first, bicarbonate helps to buffer pH until it is fully "titrated" by CO_2 removal (designated by an up arrow, shown below):

$$2HCO_3^- \rightleftharpoons CO_2(\uparrow) + H_2O + CO_3^{-2}$$
 (10)







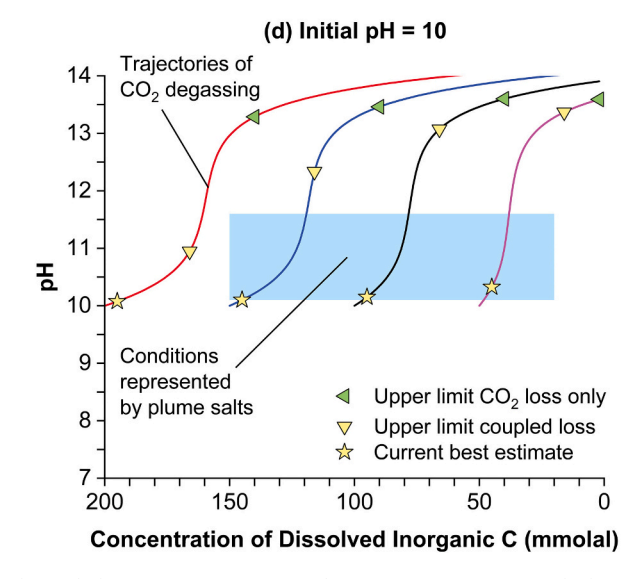


Fig. 4. Effects of CO_2 degassing on the pH of a nominal Enceladus salt solution. In each panel, the pH starts at a certain value (7, 8, 9, or 10 at 0 °C and 1 bar), and a family of trajectories can be followed depending on the initial DIC concentration (curves start at 200, 150, 100, or 50 mmolal DIC). The horizontal axis is reversed so that CO_2 is removed from left to right. The blue region demarcates the constrained conditions of final solutions. Triangles signify upper limits on CO_2 loss (and pH) for each curve based on two endmembers of material loss described in Sections 3.3.1 and 3.3.2. A trajectory is allowed if it crosses into the blue region before reaching the triangle of interest. Yellow stars show the amount of CO_2 loss in our preferred scenario of coupled loss of CO_2 and salt solutions, with steam condensation fixed by the observed heat flux. (For interpretation of the references to color in this figure legend, the reader is referred to the web version of this article.)

and then, pH increases steeply due to the formation of hydroxide:

$$CO_3^{-2} + H_2O \Rightarrow CO_2(\uparrow) + 2OH^-$$
 (11)

Was the initial pH before degassing significantly lower than the apparent pH? If the amount of degassing is treated as a free parameter, then the pH could have started at values down to 7 (Fig. 4a), or possibly lower. Fortunately, we can use the measured abundance of CO₂ as a constraint. We develop two endmember models in an attempt to bound the possibilities. We call these models "perfectly coupled loss" (yellow triangles in Fig. 4) and "CO2 loss only" (green triangles). In the former model, CO2 is lost together with its host solution. This model (Fig. 3) seems to resemble the plume, which contains both gases and salty grains (i.e., frozen host solutions). The erupted material would preserve the bulk composition of the source fluid. However, we cannot dismiss the possibility that gases may be preferentially lost since we do not know a priori the dissolved gas content of the source water. While the plume is known to contain salty grains, it could have a larger ratio of CO₂-to-salts compared with the ocean below. Thus, it seems wise to also consider an endmember of CO₂ loss only. Below, we constrain the loss of CO₂ for these scenarios.

3.3.1. Perfectly coupled loss of CO2 and salt water

3.3.1.1. Most conservative case. If perfectly coupled loss occurs, each kilogram of liquid water going into space would degas CO_2 and H_2O into some volume. Because both species enter the same "headspace," their molar quantities (n) and partial pressures follow a simple relationship:

$$\frac{n_{\text{CO}_2,\text{LVE}}}{n_{\text{H}_2\text{O},\text{LVE}}} = \frac{p_{\text{CO}_2,\text{LVE}}}{p_{\text{H}_2\text{O},\text{LVE}}}$$
(12)

As described in Section 3.2, $p_{\rm H_2O,LVE} \approx 0.0061$ bar and $p_{\rm CO_2,LVE} \leq 10^{-4.5}$ bar. The amount of water vapor that will be produced can be determined by setting an energy balance between the latent heats of fusion ($\Delta H_{\rm fus}$) and vaporization ($\Delta H_{\rm vap}$) of water at triple-point conditions. The fraction of water vaporized ($f_{\rm vap}$) is therefore given by

$$f_{\text{vap}} = \frac{\Delta H_{\text{fus}}}{\Delta H_{\text{fus}} + \Delta H_{\text{vap}}} = \frac{6.01 \text{ kJ/mol}}{6.01 + 45.06} = 0.118$$
 (13)

Each kilogram of liquid water contains \sim 55.5 mol, so \sim 6.55 mol of water vapor will be produced. Using the above values, we can calculate the amount of CO₂ via Eq. (12). We find that at most \sim 34 mmol CO₂/kg liquid water could be degassed.

3.3.1.2. Current best estimate. The preceding upper limit corresponds to a case with no water vapor condensation in Enceladus's tiger stripes. However, there are grains of almost pure ice being erupted (Postberg et al., 2009) and substantial thermal emission from the tiger stripes (Spencer et al., 2006). The deposition of water from gas to solid can explain both observations (Schmidt et al., 2008; Nakajima and Ingersoll, 2016). The rate of deposition ($D_{\rm H_2O}$) can be calculated via another energy balance that assumes that the radiant flux emitted by the tiger stripes ($\Phi_{\rm tiger}$; Spencer et al., 2018) comes from the deposition of water vapor (i.e., the reverse of sublimation). We find that

$$D_{\rm H_2O} \approx \frac{\Phi_{\rm tiger}}{\Delta \rm H_{\rm sub}} \approx \frac{4.2 \times 10^9 \text{ W}}{2.83 \times 10^6 \text{ J/kg}} \approx 1500 \text{ kg/s} \tag{14}$$

It is then simple to estimate the amount of water vapor remaining in the plume gas compared with the amount originally vaporized from liquid water. The ratio can be expressed as

$$\frac{\dot{n}_{\rm H_2O,SVE}}{\dot{n}_{\rm H_2O,LVE}} = \frac{L_{\rm H_2O}}{L_{\rm H_2O} + D_{\rm H_2O}} \approx \frac{300}{300 + 1500} \approx 0.17 \tag{15}$$

where the loss rate of water vapor ($L_{\rm H_2O}$ in kg/s) is from Hansen et al.

(2020). Inserting the above result into Eq. (9) yields $p_{\text{CO}_2,\text{LVE}} \approx 10^{-5.3}$ bar, which corresponds to degassing of ~ 5 mmol CO₂/kg liquid water. This is our preferred scenario. If we speciate the two endmembers of salinity shown in Table S1 with this value of $p_{\text{CO}_2,\text{LVE}}$, we obtain a pH of 10.6–10.7—remarkably consistent with the range (10.1–11.6) independently estimated from the phosphate speciation (Fig. 2).

Note that Fifer et al. (2022) estimated that \sim 60–70 % of water vapor should condense during transport, which is similar (and essentially identical on a logarithmic scale; see Eq. 9) to our value of \sim 83 % (see Eq. 15). Thus, the large difference between pH values boils down to how the two models treat the liquid-vapor interface. We assume that gases equilibrate between the two phases (or at least get close to equilibrium), whereas Fifer et al. (2022) assumed that transport from the liquid to the gas phase is kinetically controlled.

 ${\rm CO_2}$ condensation (Combe et al., 2019) would lead to a higher model-derived pH compared with the actual pH (Glein et al., 2015). However, this process may not significantly affect our derivation of pH because only ${\sim}83$ % of water vapor is expected to freeze out, and ${\rm CO_2}$ is far less condensable than ${\rm H_2O}$ is. For context, ${\rm CO_2}$ ice has a vapor pressure that is larger than that of ${\rm H_2O}$ ice by a factor of ${\rm 10^6}$ at 200 K (Huber et al., 2022). This temperature is comparable to that (177–217 K) determined by Goguen et al. (2013) after Cassini's infrared mapper peered into one of Enceladus's tiger stripes (Baghdad Sulcus). It might serve as a reasonable estimate for the final point of solid-vapor equilibrium prior to plume formation (Fig. 3). We suspect that only a small fraction (<1 %) of ${\rm CO_2}$ may condense inside Enceladus's tiger stripes because they are too warm.

3.3.2. CO₂ loss with retention of salt water inside Enceladus

Alternatively, we can consider Enceladus's ocean to be a finite reservoir that simply loses CO₂, causing the remaining DIC concentration to decrease through time. The change in DIC molality due to outgassing can be related to the loss rate of CO₂ from the plume ($L_{\rm CO_2}\approx 2.6\times 10^9\,{\rm mol/yr}$; Hansen et al., 2020; Peter et al., 2024), as shown below:

$$\Delta m_{\rm DIC} \approx -\frac{L_{\rm CO_2} \tau_{\rm out}}{M_{\rm oc}} \tag{16}$$

where M_{oc} stands for the mass of the ocean ($\sim 1.3 \times 10^{19}$ kg; Park et al., 2024), and τ_{out} designates the outgassing timescale. Hörst et al. (2008) proposed that CO in Titan's atmosphere is sourced by O⁺ ultimately derived from water in Enceladus's plume. They calculated that it would take ~ 300 Myr for CO to build up to the level now observed. We suggest that this process could date the duration of plume activity (it may also provide a constraint on the age of Enceladus; see Nimmo et al., 2023), giving us $\Delta m_{\rm DIC} \approx -60$ mmol CO₂/kg liquid water from Eq. (16). However, this value is probably an upper limit on CO₂ loss for two reasons: (1) Carbonate minerals on the seafloor of Enceladus should dissolve within this timeframe (Hao et al., 2022), helping to restore DIC; and (2) If some of Titan's CO is primordial or was delivered by comets, then less CO production would be implied.

3.3.3. Synthesis: Insignificant evolution of pH

The above constraints on the amount of CO_2 degassing can be used to restrict the parameter space of pH-DIC conditions of pristine ocean water. The fewest restrictions come from our model of CO_2 loss only. In this case, the initial pH could be 7 (or lower) but only if the initial DIC concentration is less than ~ 120 mmolal (Fig. 4a). The initial pH can be 10 (or higher) provided that a trajectory is chosen that ends inside the blue box (Fig. 4d). However, " CO_2 loss only" may not be realistic (Fig. 3). Ocean water with a pH of 10 is susceptible to a big jump in pH with the loss of CO_2 because most (~ 60 %) of its DIC is in the forms of $NaCO_3^-$ and CO_3^{-2} . These carbonate species can easily generate a significant amount of OH^- . In contrast, starting solutions with lower pH

values and high DIC concentrations, in particular, have more base-buffering capacity. Assuming that "coupled loss" is more realistic, then an initial pH of 7 would be inconsistent with the inferred pH range unless the initial DIC concentration is relatively low (<70 mmolal; Fig. 4a). Yet, such a low DIC concentration may not be sufficient to drive the release of abundant phosphate from minerals (Postberg et al., 2023). While we cannot rule out a circumneutral pH for Enceladus's ocean, we consider it unlikely. Our preferred model of outgassing (indicated by stars in Fig. 4) predicts small changes in DIC concentration and pH. A minimal extent (<0.2 units) of pH evolution during degassing means that the pH of plume salt solutions should be representative of pristine ocean water (see Section 4.3).

4. Implications

4.1. Water-rock interactions create alkaline ocean water

Our new understanding of the pH of Enceladus's ocean and how volatile signatures are transferred between the ocean and plume have important implications. High pH ocean water is evidence of a strong degree of interaction between chemically basic rocks and the ocean of Enceladus (Glein et al., 2015). Aqueous alteration (e.g., serpentinization) of Mg- and Fe(II)-rich silicates, such as those found in carbonaceous asteroids (Nakamura et al., 2023; Lauretta et al., 2024), is one possibility. Another possibility is the alteration of peralkaline rocks with molar Na/Al > 1. Refractory cometary grains appear to be peralkaline (Bardyn et al., 2017). The alteration of such material would release excess NaOH into solution, which after reacting with CO₂, may be responsible for a high alkalinity of sodium carbonates (Postberg et al., 2009, 2021).

If Enceladus's core contains rocks similar to dust observed from comet 67P, then this bulk composition may allow much higher concentrations of DIP to exist than those predicted for chemical equilibrium between liquid water and chondritic rocks (Randolph-Flagg et al., 2023). A key distinction is the Na/Al ratio, which is below unity in carbonaceous chondrites (Lodders, 2021). In saponite (e.g., Na_{0,33}Mg₃₋ $Si_{3.67}Al_{0.33}O_{10}(OH)_2)$, an abundant secondary mineral in aqueously altered chondrites (Lee et al., 2025), substitution of Si by Al in tetrahedral sites enables a corresponding amount of Na to be incorporated into the interlayer space. This incorporation makes it more difficult to release Na into aqueous solution. When the rock is peralkaline, however, Na cannot be completely charge-balanced by Al in stable aluminosilicates. Thus, Na is more prone to leaching and can go on to react with accreted CO2, producing a solution with high pH and high carbonate alkalinity. The latter quantity increases the solubilities of phosphate minerals (Hao et al., 2022). We note that these are our expectations, and that this type of alteration has not been modeled yet for Enceladus's ocean.

4.2. How strong is the evidence for hydrothermal silica?

A second implication of this work is that a high ocean pH adds to a body of evidence that may question the interpretation of silica (SiO₂) nanoparticles as indicators of the cooling of hydrothermal fluids inside Enceladus (Hsu et al., 2015). It was argued that forming and maintaining these particles requires a pH between 8.5 and 10.5. At higher pH, colloidal silica is too soluble. Our estimated pH range (10.1–11.6) is marginally consistent with the proposed solubility limit. The hypothesis of hydrothermal silica also has other problems. First, it is challenging to find conditions that permit the coexistence of high SiO_2 and H_2 abundances. Silica inhibits H_2 production by stabilizing ferrous iron in silicate minerals, rather than supporting the oxidation of iron by water (e. g., Sleep et al., 2004). Chemical heterogeneity of Enceladus's core may need to be invoked to reconcile current interpretations for SiO_2 and H_2 (Glein et al., 2018). Finally, modeling of ocean circulation suggests that transport times from the bottom to the top of Enceladus's ocean are

probably too long to allow silica nanoparticles to survive this passage (Zeng and Jansen, 2021; Kang et al., 2022; Ames et al., 2025; see Schoenfeld et al., 2023; Bouffard et al., 2025). It seems hard to understand how such particles would not grow/dissolve before being embedded in plume ice grains. These findings highlight the importance of exploring alternative explanations of the silica nanoparticle data in the future.

4.3. Reconstruction of ocean chemistry from plume composition

Since the phosphate-derived pH provides a validation of our outgassing model, we now have an improved tool (see Waite et al., 2017; Fifer et al., 2022; Mitchell et al., 2024) for converting between plume gas mixing ratios and dissolved concentrations in Enceladus's ocean. As an example, here we apply our model to H₂, CH₄, and NH₃. To reconstruct the composition of the ocean, we conduct three sets of calculations. In the first set, we determine concentrations of gases that are still dissolved after degassing. While we could just use Henry's law for H₂ and CH4, a full speciation model must be run because NH3 will be in equilibrium with NH₄⁺. We adopt nominal values for the concentrations of Cl (0.2 m), DIC (0.1 m), and DIP (0.004 m), as well as previously used ratios of K/Na and Br/Cl. The pH (~10.7) is determined via charge balance based on the partial pressure of CO₂. We impose fixed partial pressures of gases from Eq. (9) with $\dot{n}_{\rm H_2O,SVE}/\dot{n}_{\rm H_2O,LVE} \approx 0.17$ (see Eq. 15) and observed mixing ratios (Waite et al., 2017; Peter et al., 2024). We speciate this system using React in GWB (with decoupled redox species) and find the following dissolved concentrations: $H_2 = 1 \times 10^{-8}$ m, CH_4 = 3×10^{-9} m, and $\Sigma NH_3 = 0.006$ m (ΣNH_3 stands for NH_3 (aq) + NH_4^+).

Next, we calculate the degassed amounts of H_2 , CH_4 , and NH_3 . A suitable equation can be derived by multiplying Eq. (7) by the number of moles of water vapor also generated during evaporative freezing, and generalizing the result:

$$\frac{n_{\text{Gas,LVE}}}{\text{kg liquid}} \approx \frac{n_{\text{H}_2\text{O,LVE}}}{\text{kg liquid}} \times \frac{\dot{n}_{\text{H}_2\text{O,SVE}}}{\dot{n}_{\text{H}_2\text{O,LVE}}} \times (\text{Gas/H}_2\text{O})_{\text{SVE}}$$
(17)

where "Gas" refers to any non-condensable gas, and Gas/ H_2O designates the molar ratio of this species with respect to water vapor. The left side of Eq. (17) signifies the molality of gas removed. In Section 3.3.1.1, we showed that $n_{H_2O,LVE}$ could be $\sim\!6.55$ mol per kilogram of liquid water. We can also adopt a value of $\sim\!0.17$ for $\dot{n}_{H_2O,SVE}/\dot{n}_{H_2O,LVE}$ (see Eq. 15). Thus

$$\frac{\text{mol Gas}}{\text{kg liquid}} \approx 1.1 \times \left(\text{Gas}/\text{H}_2\text{O}\right)_{\text{SVE}} \tag{18}$$

Based on the plume gas composition (Waite et al., 2017; Peter et al., 2024), the degassed amounts are calculated to be: $H_2 = 0.01 \, m$, $CH_4 = 0.001 \, m$, and $NH_3 = 0.02 \, m$.

The final step is to add the outgassed inventory back into the previously speciated solution and respeciate the new solution with the full volatile inventory. Such "regassing" can be simulated in React using the pickup command. We also add in the outgassed amounts of CO2 (\sim 0.005 mol/kg liquid water; see Section 3.3.1.2) and H₂O (\sim 6.55 mol/ kg liquid water; see Section 3.3.1.1). Table A1 displays the calculated ocean speciation. This output represents a nominal estimate of the inorganic chemistry of Enceladus's ocean before ocean water experiences compositional modification due to the eruptive process that forms the plume. It is tempting to call this "the ocean composition," and it may be, although a detailed analysis of the uncertainty space propagating from the input data has yet to be performed. The main point of this exercise is to demonstrate how the chemistry of the ocean can be inferred using a framework that is consistent with constraints from observations and the thermodynamics of outgassing on Enceladus. Interestingly, regassing hardly decreases the pH (<0.1 units). CO₂ degassing has the tendency to increase pH but is partly counterbalanced by NH3 degassing. They have opposing acid-base effects. This is even better

news than our finding from Section 3.3.3 because it makes us more confident that future measurements of the pH of plume ice (after collection and melting) will be representative of the underlying ocean.

Lastly, this nominal ocean composition (Table A1) can serve as a baseline for future studies, and it may motivate us to revisit some previous assumptions about the geochemistry and habitability of Enceladus. For example, could its ocean contain too much free NH3 for life (McKay et al., 2008)? Are key transition metals that are needed to produce certain biological catalysts (e.g., hydrogenases) sufficiently abundant at this high pH (Xu et al., 2025)? Could NH3 also contribute to the high pH (e.g., Leitner and Lunine, 2019)? Although our estimated pH is about two units higher than that of Fifer et al. (2022), our estimates of dissolved gas concentrations in Enceladus's ocean also support the existence of a gassy ocean, as originally suggested by Kargel (2006). However, we find that H₂ could be the dominant low-solubility gas, and free CO₂ may not be abundant as the pH is high. A high H₂ concentration drives the CO₂-CH₄ redox couple out of chemical equilibrium, and we calculate that hydrogenotrophic methanogenesis could supply ~140 kJ/ mol CH₄ of free energy below the zone of degassing in the ocean. Enceladus's ocean remains energetically habitable (Waite et al., 2017; Fifer et al., 2022). The high abundance of H₂ may also be geophysically relevant. Mitchell et al. (2024) emphasized that H2 exsolution could drive explosive cryovolcanism on Enceladus. Our geochemical model suggests that H₂ would exsolve at ~10 bars of total pressure, or at depths shallower than ~9.6 km in the ice shell of Enceladus, thus supporting a role for H₂ in Enceladus's eruption dynamics. Table A1 may incite numerous additional questions, which can help to catalyze progress in achieving a deeper understanding of Enceladus. The future looks bright. Moreover, the general capability of our model for dissolved gases may prove useful in interpreting current/future measurements of other volatiles, including certain organic compounds (e.g., MacKenzie et al., 2021).

CRediT authorship contribution statement

Christopher R. Glein: Writing – review & editing, Writing – original draft, Visualization, Validation, Project administration, Methodology, Investigation, Funding acquisition, Formal analysis, Conceptualization. Ngoc Truong: Writing – review & editing.

Declaration of competing Interest

The authors declare that they have no known competing financial interests or personal relationships that could have appeared to influence the work reported in this paper.

Acknowledgments

This work was supported by NASA's Habitable Worlds program. We thank Frank Postberg for making his group's updated plume salt numbers available to the community by presenting them at the 2021 AGU Fall Meeting. We are also grateful to two reviewers who made a number of excellent suggestions for improvements.

Appendix A. Geochemical properties of Enceladean ocean water prior to degassing

Table A1 shows results from a series of thermodynamic calculations that are described in Section 4.3. In the laboratory, this speciation can be produced by preparing an aqueous solution containing 0.158 m NaCl, 0.0180 m KCl, 0.0722 m Na₂CO₃, 0.0210 m NaHCO₃, 0.00353 m Na₂HPO₄, 0.000404 m NaBr, and 0.0255 m NH₄OH under a 10.6 bar atmosphere containing 96 mol% H₂ and 4 mol% CH₄ at 0 °C. One could test whether methanogens can grow in Enceladus's ocean.

Table A1 Nominal geochemical properties of Enceladus's ocean at 0 °C and 1 bar. Brackets indicate the concentration of the enclosed species. Molal concentrations are given down to a value of 1×10^{-9} . Organic species (Khawaja et al., 2019) are not included.

Property	Value
pH	10.6
Eh (V) ^a	-0.621
$\log f_{O_2}(\text{bar})^{\text{b}}$	-94.3
$log f_{O_2}(vs. FMQ)^c$	-5.9
$p_{\rm H_2}~{ m (bar)}^{ m d}$	10.2
$p_{\mathrm{CH_4}} \mathrm{(bar)^d}$	0.4
Ionic strength (molal)	0.333
Activity of H ₂ O	0.994
$A_{\text{CO}_2-\text{CH}_4}$ (kJ/mol CH ₄) ^e	140
[Na ⁺]	0.274
[Cl ⁻]	0.173
[NaCO ₃]	0.0482
[CO ₃ ⁻²]	0.0311
[NH ₃ (aq)] ^f	0.0181
[K ⁺]	0.0179
[HCO ₃]	0.0106
[H ₂ (aq)] ^g	0.0100
[NH4]	0.00744
[NaCl(aq)]	0.00335
[NaHCO ₃ (aq)]	0.00328
[NaHPO ₄]	0.00156
[HPO ₄ ⁻²]	0.00147
[CH ₄ (aq)] ^f	0.00100
[Br ⁻]	0.000402
[Na ₂ HPO ₄ (aq)]	0.000177
$[PO_4^{-3}]$	0.000101
	(continued on next page)

(continued on next page)

Table A1 (continued)

Property	Value
[NaPO ₄ ⁻²]	7.55e-05
$[Na_2PO_4^-]$	7.36e-05
[OH ⁻]	7.29e-05
[KHPO ₄]	5.88e-05
[NaOH(aq)]	6.27e-06
$[KPO_4^{-2}]$	4.11e-06
[KCl(aq)]	2.04e-06
[NaBr(aq)]	1.83e-06
[K ₂ HPO ₄ (aq)]	1.52e-06
[CO ₂ (aq)] ^f	6.49e-07
$[H_2PO_4^-]$	2.33e-07
[KOH(aq)]	1.68e-07
$[K_2PO_4^-]$	7.57e-08
[NaH ₂ PO ₄ (aq)]	6.39e-08
[KBr(aq)]	3.70e-08
[KH ₂ PO ₄ (aq)]	5.91e-09
$[P_2O_7^{-4}]$	2.29e-09
[H ₂ CO ₃ (aq)]	1.10e-09
2 7 1 1 1 1 1 1 1 1 1 1	11 1

^a Reduction potential relative to standard hydrogen electrode.

Appendix B. Supplementary data

Supplementary data to this article can be found online at https://doi.org/10.1016/j.icarus.2025.116717.

Data availability

Data will be made available on request.

References

Ames, F., et al., 2025. Ocean stratification impedes particulate transport to the plumes of Enceladus. Commun. Earth Environ. 6, 63. https://doi.org/10.1038/s43247-025-02026.2

Awolayo, A.N., Tutolo, B.M., 2022. PyGeochemCalc: A python package for geochemical thermodynamic calculations from ambient to deep Earth conditions. Chem. Geol. 606, 120984. https://doi.org/10.1016/j.chemgeo.2022.120984.

Bardyn, A., et al., 2017. Carbon-rich dust in comet 67P/Churyumov-Gerasimenko measured by COSIMA/Rosetta. Mon. Not. R. Astron. Soc. 469, S712–S722.

Bouffard, M., et al., 2025. Seafloor hydrothermal control over ocean dynamics in Enceladus. Nat. Astron. 9, 650–657.

Burke, S.E., et al., 2023. Detection of intact amino acids with a hypervelocity ice grain impact mass spectrometer. Proc. Natl. Acad. Sci. USA 120, e2313447120. https:// doi.org/10.1073/pnas.2313447120.

Cable, M.L., et al., 2021. The science case for a return to Enceladus. Planet. Sci. J. 2, 132. https://doi.org/10.3847/PSJ/abfb7a.

Castillo-Rogez, J.C., et al., 2022. Contribution of non-water ices to salinity and electrical conductivity in ocean worlds. Geophys. Res. Lett. 49. https://doi.org/10.1029/ 2021GL097256 e2021GL097256.

Choi, J., et al., 1998. Modeling ${\rm CO_2}$ degassing and pH in a stream-aquifer system. J. Hydrol. 209, 297–310.

Combe, J.-P., et al., 2019. Nature, distribution and origin of CO_2 on Enceladus. Icarus 317. 491–508.

Daniele, P.G., et al., 1991. Salt effects on the protonation of ortho-phosphate between 10 and 50°C in aqueous solution. A complex formation model. J. Solut. Chem. 20, 495–515.

Fifer, L.M., et al., 2022. Chemical fractionation modeling of plumes indicates a gas-rich, moderately alkaline Enceladus ocean. Planet. Sci. J. 3, 191. https://doi.org/

Fox-Powell, M.G., Cousins, C.R., 2021. Partitioning of crystalline and amorphous phases during freezing of simulated Enceladus ocean fluids. J. Geophys. Res. Planets 126. https://doi.org/10.1029/2020JE006628 e2020JE006628. Glavin, D.P., et al., 2025. Abundant ammonia and nitrogen-rich soluble organic matter in samples from asteroid (101955) Bennu. Nat. Astron. 9, 199–210.

Glein, C.R., Waite, J.H., 2020. The carbonate geochemistry of Enceladus' ocean.
 Geophys. Res. Lett. 47. https://doi.org/10.1029/2019GL085885 e2019GL085885.
 Glein, C.R., et al., 2015. The pH of Enceladus' ocean. Geochim. Cosmochim. Acta 162, 202–219.

Glein, C.R., et al., 2018. The geochemistry of Enceladus: Composition and controls. In: Schenk, P.M., et al. (Eds.), Enceladus and the Icy Moons of Saturn. Univ. of Arizona Press, Tucson, AZ, pp. 39–56.

Goguen, J.D., et al., 2013. The temperature and width of an active fissure on Enceladus measured with Cassini VIMS during the 14 April 2012 South Pole flyover. Icarus 226, 1128–1137.

Hansen, C.J., et al., 2006. Enceladus' water vapor plume. Science 311, 1422–1425.

Hansen, C.J., et al., 2020. The composition and structure of Enceladus' plume from the complete set of Cassini UVIS occultation observations. Icarus 344, 113461. https://doi.org/10.1016/j.icarus.2019.113461.

Hao, J., et al., 2022. Abundant phosphorus expected for possible life in Enceladus's ocean. Proc. Natl. Acad. Sci. USA 119, e2201388119. https://doi.org/10.1073/ pnas.2201388119.

Helgeson, H.C., 1969. Thermodynamics of hydrothermal systems at elevated temperatures and pressures. Am. J. Sci. 267, 729–804.

Holland, T.J.B., Powell, R., 2011. An improved and extended internally consistent thermodynamic dataset for phases of petrological interest, involving a new equation of state for solids. J. Metamorph. Geol. 29, 333–383.

Hörst, S.M., et al., 2008. Origin of oxygen species in Titan's atmosphere. J. Geophys. Res. Planets 113, E10006. https://doi.org/10.1029/2008JE003135.

Hsu, H.-W., et al., 2015. Ongoing hydrothermal activities within Enceladus. Nature 519, 207–210.

Huang, F., Sverjensky, D.A., 2019. Extended Deep Earth Water Model for predicting major element mantle metasomatism. Geochim. Cosmochim. Acta 254, 192–230.

Huber, M.L., et al., 2022. The NIST REFPROP database for highly accurate properties of industrially important fluids. Ind. Eng. Chem. Res. 61, 15449–15472.

Jin, Q., Kirk, M.F., 2018. pH as a primary control in environmental microbiology: 1. Thermodynamic perspective. Front. Environ. Sci. 6, 21. https://doi.org/10.3389/fenvs.2018.00021.

Kang, W., et al., 2022. Ocean dynamics and tracer transport over the south pole geysers of Enceladus. Mon. Not. R. Astron. Soc. 517, 3485–3494.

Kargel, J.S., 2006. Enceladus: cosmic gymnast, volatile miniworld. Science 311, 1389–1391.

^b Oxygen fugacity.

^c Fayalite-magnetite-quartz buffer based on thermodynamic data from Holland and Powell (2011).

^d Equilibrium partial pressure.

 $[^]e$ Chemical affinity for CO2(aq) $+\ 4H_2(aq)\to$ CH4(aq) $+\ 2H_2O(liq),$ which quantifies how far this reaction is from chemical equilibrium.

^f Dissolved concentration based on plume gas data from Peter et al. (2024).

^g Dissolved concentration based on plume gas data from Waite et al. (2017).

- Khawaja, N., et al., 2019. Low-mass nitrogen-, oxygen-bearing, and aromatic compounds in Enceladean ice grains. Mon. Not. R. Astron. Soc. 489, 5231–5243.
- Klenner, F., et al., 2019. Analogue spectra for impact ionization mass spectra of water ice grains obtained at different impact speeds in space. Rapid Commun. Mass Sp. 33, 1751–1760.
- Lauretta, D.S., et al., 2024. Asteroid (101955) Bennu in the laboratory: properties of the sample collected by OSIRIS-REx. Meteorit. Planet. Sci. 59, 2453–2486.
- Lee, M.R., et al., 2025. Low-temperature aqueous alteration of chondrites. Space Sci. Rev. 221, 11. https://doi.org/10.1007/s11214-024-01132-8.
- Leitner, M.A., Lunine, J.I., 2019. Modeling early Titan's ocean composition. Icarus 333, 61–70.
- Lodders, K., 2021. Relative atomic solar system abundances, mass fractions, and atomic masses of the elements and their isotopes, composition of the solar photosphere, and compositions of the major chondritic meteorite groups. Space Sci. Rev. 217, 44. https://doi.org/10.1007/s11214-021-00825-8.
- MacKenzie, S.M., et al., 2021. The Enceladus Orbilander mission concept: balancing return and resources in the search for life. Planet. Sci. J. 2, 77. https://doi.org/ 10.3847/PSJ/abe4da.
- Matsumoto, T., et al., 2024. Sodium carbonates on Ryugu as evidence of highly saline water in the outer Solar System. Nat. Astron. 8, 1536–1543.
- McCleskey, R.B., et al., 2012. A new method of calculating electrical conductivity with applications to natural waters. Geochim. Cosmochim. Acta 77, 369–382.
- McCoy, T.J., et al., 2025. An evaporite sequence from ancient brine recorded in Bennu samples. Nature 637, 1072–1077.
- McKay, C.P., et al., 2008. The possible origin and persistence of life on Enceladus and detection of biomarkers in the plume. Astrobiology 8, 909–919.
- Mitchell, K.L., et al., 2024. A proposed model for cryovolcanic activity on Enceladus driven by volatile exsolution. J. Geophys. Res. Planets 129. https://doi.org/ 10.1029/2023JE007977 e2023JE007977.
- Nakajima, M., Ingersoll, A.P., 2016. Controlled boiling on Enceladus. 1. Model of the vapor-driven jets. Icarus 272, 309–318.
- Nakamura, T., et al., 2023. Formation and evolution of carbonaceous asteroid Ryugu: direct evidence from returned samples. Science 379, eabn8671. https://doi.org/ 10.1126/science.abn8671.
- Nimmo, F., et al., 2023. Origin and evolution of Enceladus's tidal dissipation. Space Sci. Rev. 219, 57. https://doi.org/10.1007/s11214-023-01007-4.
- Park, R.S., et al., 2024. The global shape, gravity field, and libration of Enceladus. J. Geophys. Res. Planets 129. https://doi.org/10.1029/2023JE008054 e2023JE008054.
- Peter, J.S., et al., 2024. Detection of HCN and diverse redox chemistry in the plume of Enceladus. Nat. Astron. 8, 164–173.
- Porco, C.C., et al., 2006. Cassini observes the active south pole of Enceladus. Science 311, 1393–1401.
- Postberg, F., et al., 2009. Sodium salts in E-ring ice grains from an ocean below the surface of Enceladus. Nature 459, 1098–1101.
- Postberg, F., et al., 2011. A salt-water reservoir as the source of a compositionally stratified plume on Enceladus. Nature 474, 620–622.
- Postberg, F., et al., 2018. Macromolecular organic compounds from the depths of Enceladus. Nature 558, 564–568.
- Postberg, F., et al., 2021. Compositional heterogeneity of salt-rich grains emitted from Enceladus subsurface ocean. AGU Fall Meeting, held in New Orleans, LA, 13–17

- December 2021, id. P32A-05. https://ui.adsabs.harvard.edu/abs/2021AGUFM. P32A..05P.
- Postberg, F., et al., 2023. Detection of phosphates originating from Enceladus's ocean. Nature 618, 489–493.
- Ramírez-Cabañas, A.K., et al., 2024. Exploring the general chemistry of the core and ocean of Enceladus. Adv. Space Res. 74, 480–489.
- Randolph-Flagg, N.G., et al., 2023. Phosphate availability and implications for life on ocean worlds. Nat. Commun. 14, 2388. https://doi.org/10.1038/s41467-023-37770-9
- Ray, C., et al., 2021. Oxidation processes diversify the metabolic menu on Enceladus. Icarus 364, 114248. https://doi.org/10.1016/j.icarus.2020.114248.
- Saur, J., et al., 2024. Analysis of Enceladus's time-variable space environment to magnetically sound its interior. Planet. Sci. J. 5, 245. https://doi.org/10.3847/PSJ/ ad8130.
- Schmidt, J., et al., 2008. Slow dust in Enceladus' plume from condensation and wall collisions in tiger stripe fractures. Nature 451, 685–688.
- Schoenfeld, A.M., et al., 2023. Particle entrainment and rotating convection in Enceladus' ocean. Commun. Earth Environ. 4, 28. https://doi.org/10.1038/s43247-023-00674-z.
- Seaton, K.M., et al., 2025. Replicating flyby sampling of salty ocean world ice grains in the laboratory. Lunar Planet. Sci. Conf. 56, 2464.
- Shock, E.L., et al., 1989. Calculation of the thermodynamic and transport properties of aqueous species at high pressures and temperatures: standard partial molal properties of inorganic neutral species. Geochim. Cosmochim. Acta 53, 2157–2183.
- Shock, E.L., et al., 1997. Inorganic species in geologic fluids: correlations among standard molal thermodynamic properties of aqueous ions and hydroxide complexes. Geochim. Cosmochim. Acta 61, 907–950.
- Sleep, N.H., et al., 2004. H₂-rich fluids from serpentinization: geochemical and biotic implications. Proc. Natl. Acad. Sci. USA 101, 12818–12823.
- Spencer, J.R., et al., 2006. Cassini encounters Enceladus: background and the discovery of a south polar hot spot. Science 311, 1401–1405.
- Spencer, J.R., et al., 2018. Plume origins and plumbing: From ocean to surface. In: Schenk, P.M., et al. (Eds.), Enceladus and the Icy Moons of Saturn. Univ. of Arizona Press, Tucson, AZ, pp. 163–174.
- Thomas, P.C., et al., 2016. Enceladus's measured physical libration requires a global subsurface ocean. Icarus 264, 37–47.
- Villanueva, G.L., et al., 2023. JWST molecular mapping and characterization of Enceladus' water plume feeding its torus. Nat. Astron. 7, 1056–1062.
- Waite, J.H., et al., 2009. Liquid water on Enceladus from observations of ammonia and ⁴⁰Ar in the plume. Nature 460, 487–490.
- Waite, J.H., et al., 2017. Cassini finds molecular hydrogen in the Enceladus plume: evidence for hydrothermal processes. Science 356, 155–159.
- Xu, W., et al., 2025. Enough sulfur and iron for potential life make Enceladus's ocean fully habitable. Astrophys. J. Lett. 980, L10. https://doi.org/10.3847/2041-8213/ adad65.
- Zeng, Y., Jansen, M.F., 2021. Ocean circulation on Enceladus with a high- versus low-salinity ocean. Planet. Sci. J. 2, 151. https://doi.org/10.3847/PSJ/ac1114.
- Zolotov, M.Y., 2007. An oceanic composition on early and today's Enceladus. Geophys. Res. Lett. 34, L23203. https://doi.org/10.1029/2007GL031234.